






Brief Report

Zweifach–Fung Microfluidic Device for Efficient Microparticle Separation: Cost-Effective Fabrication Using CO₂ Laser-Ablated PMMA

Cristian F. Rodríguez ^{1,2} , Mateo Báez-Suárez ¹, Carolina Muñoz-Camargo ¹ , Luis H. Reyes ³ ,
Johann F. Osma ^{1,4}  and Juan C. Cruz ^{1,3,*} 

¹ Department of Biomedical Engineering, Universidad de los Andes, Cra. 1E No. 19a-40, Bogotá 111711, Colombia; cf.rodriguez@uniandes.edu.co (C.F.R.); m.baezs@uniandes.edu.co (M.B.-S.); c.munoz2016@uniandes.edu.co (C.M.-C.); jf.osma43@uniandes.edu.co (J.F.O.)

² Neuroscience Group of Antioquia, Cellular and Molecular Neurobiology Area, School of Medicine, SIU, University of Antioquia, Cl. 62 No. 52-59, Medellín 050010, Colombia

³ Grupo de Diseño de Productos y Procesos (GDPP), Department of Chemical Engineering, Universidad de los Andes, Cra. 1E No. 19a-40, Bogotá 111711, Colombia; lh.reyes@uniandes.edu.co

⁴ Department of Electrical and Electronic Engineering, Universidad de los Andes, Cra. 1E No. 19a-40, Bogotá 111711, Colombia

* Correspondence: jc.cruz@uniandes.edu.co

Abstract: Microfluidic separators play a pivotal role in the biomedical and chemical industries by enabling precise fluid manipulations. Traditional fabrication of these devices typically requires costly cleanroom facilities, which limits their broader application. This study introduces a novel microfluidic device that leverages the passive Zweifach–Fung principle to overcome these financial barriers. Through Lagrangian computational simulations, we optimized an eleven-channel Zweifach–Fung configuration that achieved a perfect 100% recall rate for particles following a specified normal distribution. Experimental evaluations determined 2 mL/h as the optimal total flow rate (TFR), under which the device showcased exceptional performance enhancements in precision and recall for micrometer-sized particles, achieving an overall accuracy of 94% ± 3%. Fabricated using a cost-effective, non-cleanroom method, this approach represents a significant shift from conventional practices, dramatically reducing production costs while maintaining high operational efficacy. The cost of each chip is less than USD 0.90 cents and the manufacturing process takes only 15 min. The development of this device not only makes microfluidic technology more accessible but also sets a new standard for future advancements in the field.

Keywords: labs-on-a-chip; microfluidic-device; microparticle-separator; COMSOL; low-cost; SWOT



Citation: Rodríguez, C.F.; Báez-Suárez, M.; Muñoz-Camargo, C.; Reyes, L.H.; Osma, J.F.; Cruz, J.C. Zweifach–Fung Microfluidic Device for Efficient Microparticle Separation: Cost-Effective Fabrication Using CO₂ Laser-Ablated PMMA. *Micromachines* **2024**, *15*, 932. <https://doi.org/10.3390/mi15070932>

Received: 17 June 2024

Revised: 17 July 2024

Accepted: 19 July 2024

Published: 22 July 2024



Copyright: © 2024 by the authors. Licensee MDPI, Basel, Switzerland. This article is an open access article distributed under the terms and conditions of the Creative Commons Attribution (CC BY) license (<https://creativecommons.org/licenses/by/4.0/>).

1. Introduction

Microfluidic devices, commonly known as Labs-on-a-Chip (LOCs), are transforming our ability to manipulate fluids at the microscale [1–3]. These devices offer substantial benefits across various fields, significantly advancing experimental methodologies by reducing the volume of chemicals and materials needed, thereby promoting sustainability and efficiency [4,5]. Enhanced heat and mass transfer rates at the microscale enable quicker experimental processes, boosting overall experimental throughput [6,7]. Moreover, microfluidics maintains steadier conditions during operations, ensuring that results are both reliable and reproducible, contrasting favorably with traditional methods [8,9].

LOCs have become indispensable in industries such as chemical production and pharmaceuticals due to their capacity for executing complex processes [10–12]. Within the confines of these microscale systems, it is possible to conduct a variety of processes with unprecedented precision and efficiency [13,14]. These processes encompass the synthesis, analysis, separation, and purification of materials, ranging from nano to micrometer

scales [15–18]. The ability to perform such intricate operations on a microscale not only enhances the quality and specificity of the outcomes but also significantly reduces the time and resources required for their completion. Such efficiency and versatility underline the growing interest in LOC technology for developing innovative solutions in chemical synthesis, pharmaceutical research, and the production of highly purified materials [19].

In the field of microfluidics, devices for the purification of materials at nano and micro scales have evolved into two broad categories: active and passive systems. Active microfluidic separators utilize external forces such as electrical, magnetic, or acoustic energies to manipulate and sort the particles within microchannels [20–23]. These techniques offer precise control, allowing for the separation based on specific physical properties of the particles.

Conversely, passive microfluidic separators leverage the inherent physical properties of fluids and particles, alongside sophisticated channel designs, to achieve separation. These methods harness intrinsic physical forces—gravity, diffusion, inertia, and hydrodynamics—without the need for external energy sources, making the precise control of channel geometry a critical factor for efficient separation [24–27].

A notable passive separation technique in microfluidics is the Zweifach–Fung effect, first described by Y.C. Fung and B.W. Zweifach in their foundational study “Microcirculation: mechanics of blood flow in capillaries” at the University of California [28]. They meticulously documented the dynamic behavior of particulate suspensions at asymmetric bifurcations within microchannels. Their observations revealed a distinct divergence in the volume fraction of particles at these points, leading to unequal distributions among the daughter branches.

Their research detailed how particle suspensions behave differently at asymmetric bifurcations within microchannels, leading to varied particle distribution across the branches, a principle crucial for precise particle sorting [29]. This mechanism has been integrated into the design of microfluidic devices that aim to achieve exact particle distribution, essential for the functionalities of LOC applications [30].

Traditional methods for manufacturing microfluidic devices typically require cleanroom facilities. However, in recent decades, there has been a notable shift towards developing novel, cost-effective approaches that do not rely on a cleanroom environment [31–34]. One prominent approach involves the use of thermoplastics, which have gained increasing popularity in the field due to their numerous advantages [35,36].

Thermoplastics offer several benefits, including faster production times and lower costs, making them highly suitable for scaling up the manufacturing process of microfluidic devices [37,38]. Among the various thermoplastics that have garnered significant interest in recent years are Cyclic Olefin Copolymers (COCs), Polypropylene (PP), Polystyrene (PS), Polycarbonate (PC), Polyethylene terephthalate (PET), Polyimide (PI), and Poly (methyl methacrylate) (PMMA) [39–45].

PMMA, in particular, has attracted increasing attention, for its unique properties, such as high transparency, biocompatibility, and easy manipulation [46–49]. This surge in interest can be attributed, in part, to the work reported by Klank et al. in 2002, which studied the manufacture of microfluidic PMMA using CO₂-laser micromachining as a rapid and cost-effective alternative for manufacturing microfluidic devices [49]. Since the publication of the article by Klank et al., various microfluidics devices have been manufactured using the CO₂-laser micromachining technique [50,51]. These devices have been applied in diverse areas such as droplet generation, micromixing, and micro-separation [52–56]. Specifically, different microfluidic separators have been developed using principles such as inertial separation, pinched flow fractionation, and deterministic lateral displacement.

However, there are a few instances of microfluidic devices employing the Zweifach–Fung effect being manufactured using laser ablation in PMMA, and in particular those with channels smaller than 100 µm [57,58]. Given the broad application potential of laser ablation in microfluidics, there is significant interest in exploring the feasibility of

using this technique to fabricate devices based on the Zweifach–Fung effect, especially for microparticle separation [59–61].

To address this challenge, we present the development of a passive microfluidic device based on the Zweifach–Fung principle, fabricated using an economical laser ablation technique in polymethyl methacrylate (PMMA), thereby circumventing the need for a cleanroom. By demonstrating the feasibility of this approach, we aim to reduce economic barriers and broaden the accessibility and application of microfluidic devices, fostering greater innovation in the field.

2. Materials and Methods

2.1. Materials

Hexane (99%), Glutaraldehyde (25%), Tween 80, and mineral oil were purchased from Sigma–Aldrich (St. Louis, MO, USA). Polymethyl methacrylate (PMMA) sheets of 2 mm and 4 mm thickness were purchased from local distributors (Bogotá, Colombia).

2.2. Computational Modeling of Microparticle Separation Dynamics

The dynamics of microparticle separation within microfluidic devices was analyzed using a Lagrangian approach in COMSOL Multiphysics 6.2 software (COMSOL Inc., Stockholm, Sweden). This method, known as particle tracing, allowed for an analysis of the effect of the flow and the magnetic field on the particle trajectories.

The flow behavior was modeled based on the fundamental principles of fluid dynamics under laminar flow conditions, governed by the Navier–Stokes equations for momentum conservation and the continuity equation for mass conservation [62,63]. These are represented as Equation (1) for the Navier–Stokes equations and Equation (2) for the continuity equation.

$$\rho(u \cdot \nabla)u = \nabla \cdot \left[-pI + \mu(\nabla u + (\nabla u)^T) \right] + F \quad (1)$$

$$\rho \nabla \cdot u = 0 \quad (2)$$

where ρ is the fluid density, u is the fluid velocity, p is the fluid pressure, I is the identity matrix, and F is the external forces. The particle tracking was performed using the Lagrangian approximation. This method relies on the assumption that particle motion can be described by Newton’s second law, which is encapsulated in Equation (3). This equation provides a framework for analyzing how forces affect particle trajectories in microfluidic devices.

$$Ft = \frac{d(m_p * v)}{dt} \quad (3)$$

where Ft is the sum of all forces acting on the particles, v is the particle velocity, and m_p is the particle mass. The influence of the fluid on the particles within the microfluidic device was quantitatively modeled by incorporating the drag force, as dictated by Stokes’ Drag Law. This fundamental force is described by Equation (4).

$$Fd = (u - v) * \frac{m_p}{\tau_p} \quad (4)$$

where u is the velocity field, v is the particle velocity, m_p is the particle mass, and τ_p is the particle velocity response time or Lagrangian time scale (Equation (5)).

$$\tau_p = \frac{p_p * d_p^2}{18\mu} \quad (5)$$

where μ is the viscosity, p_p is the particle density, and d_p is the particle diameter.

2.3. Simulation Specifics and Particle Properties

Simulations were meticulously crafted based on the unique properties of the particles used, including densities and diameters of polystyrene and chitosan. This approach ensured precise and relevant analysis for each test scenario.

These properties were modeled using a normal distribution probability density function, represented by Equation (6), and the simulations were carried out over 25 iterations.

$$f(d_p) = \frac{1}{\sigma\sqrt{2\pi}} e^{-\frac{1}{2}\left(\frac{d_p - \mu}{\sigma}\right)^2} \quad (6)$$

where d_p is the diameter of the particle, μ is the mean diameter of the particle, and σ is the standard deviation. The specifics of the means and standard deviations are detailed in Table S1. During the simulations, particles were introduced into the system at a consistent rate of 100 every 0.1 s, ensuring uniform conditions for analysis.

For chitosan microparticles, the size distribution was aligned with the results from our experimental tests, as previously documented [64]. This alignment was intended to maintain the consistency of evaluation metrics used in earlier studies, thereby ensuring comparability and methodological continuity.

2.4. Discretization and Solvers

The computational domain within the microfluidic devices was discretized using triangular elements. The Zweifach–Fung passive separator was modeled using 23,573 domain elements and 2946 boundary elements. This level of discretization ensures mesh convergence, as presented in Figure S1. A comprehensive breakdown of the discretization for additional geometries that were simulated but not manufactured, along with the parameters used for the simulations, is available in Table S2. Moreover, Figure 1 (upper panel) displays the mesh configurations and boundary conditions applied in these simulations, particularly focusing on the devices that were manufactured. Figure 1, lower panel, shows an actual picture of the manufactured device before it was glued, while Figure S2 depicts the device after the gluing process.

The computational approach to solving the equations for microfluidic systems was carried out in a stepwise manner. Initially, the analysis began with a fully coupled study using the MUMPS (MULTifrontal Massively Parallel sparse direct Solver) [65–67]. This solver, which employs Gaussian factorization through a multifrontal method, is particularly adept at handling complex, coupled systems.

Upon the successful completion of the coupled study, the data generated from the CFD were integrated into the Lagrangian particle tracking model. This next phase utilized the Generalized Minimum RESidual (GMRES) solver. This iterative solver is optimal for handling the large-scale simulations required by our study, reducing memory usage and enhancing computational efficiency. The GMRES solver enhances the modeling process by iteratively constructing a Krylov subspace from the residuals of the linear system equations.

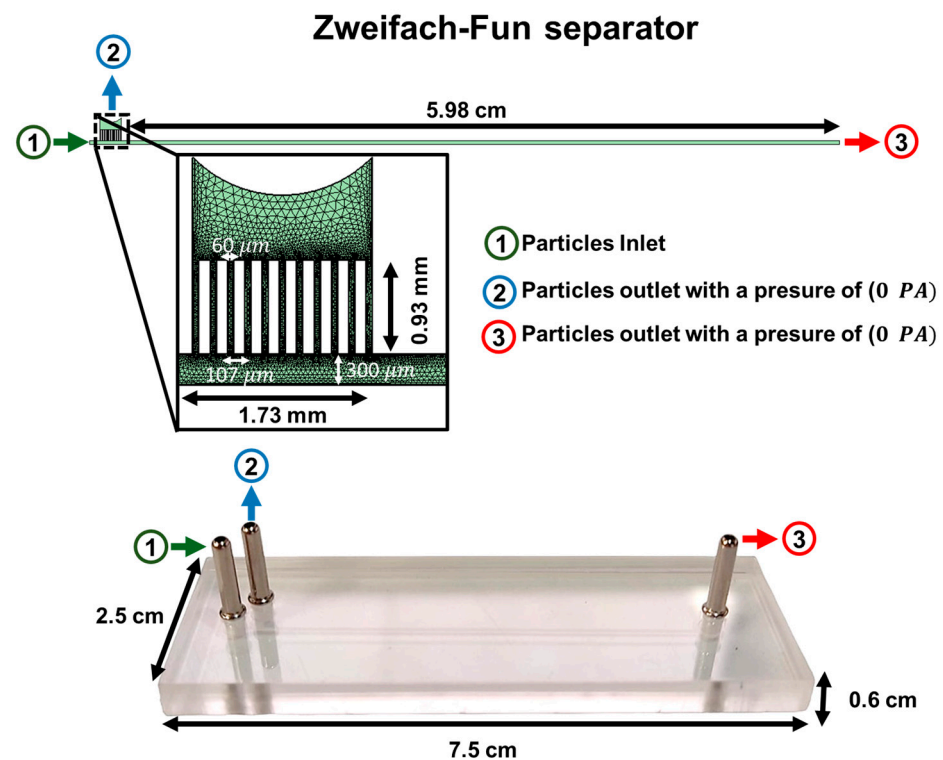


Figure 1. Meshing and boundary conditions for simulation setups for the eleven-channel Zweifach-Fung device. The microparticle inlet is indicated in green and labeled ‘1’, where particles are introduced at flow rates of 2, 20, or 200 mL/h. The outlet for particles smaller than 40 μm is marked in blue and labeled ‘2’, while the outlet for particles larger than 40 μm is highlighted in red and labeled ‘3’.

2.5. Low-Cost Manufacture

The microfluidic separator device was fabricated using an economical laser ablation method on polymethyl methacrylate (PMMA) substrates, as previously reported by Ortegon et al. [68]. Figure 2 shows graphically the manufacturing process.

The design phase involved detailed simulations using COMSOL Multiphysics 6.2 software (COMSOL Inc., Stockholm, Sweden), essential for defining the device’s geometry. This geometry was then exported to AutoCAD (AutoDesk Inc., Mill Valley, CA, USA), where the design was refined by coloring the engraving areas in black and blue and the cutting zones in red to ensure precision during the ablation process.

Following this, the PMMA sheets were processed using a TROTEC® laser cutting system (Marchtrenk, Austria). The system was set to a power of 100 and a speed of 0.4 for cutting, and a power of 15 with a speed of 12 for engraving. Afterward, the PMMA sheets underwent a thorough cleaning with a 70% ethanolic solution to remove any residual debris, ensuring a pristine surface for bonding.

The clean sheets were then bonded using a thin application of 96% ethanol and subjected to constant pressure at 110 °C for five minutes. This step was critical to ensure a strong, durable bond between the PMMA layers. The final assembly step involved accurately attaching inlets and outlets to the microfluidic device, thus equipping it for upcoming experimental applications. Figure S2 shows close-up images of the fabricated device after gluing, and Table 1 show the materials cost used for the manufacture of the microfluidic device.

Low-cost manufacturing by laser ablation in PMMA

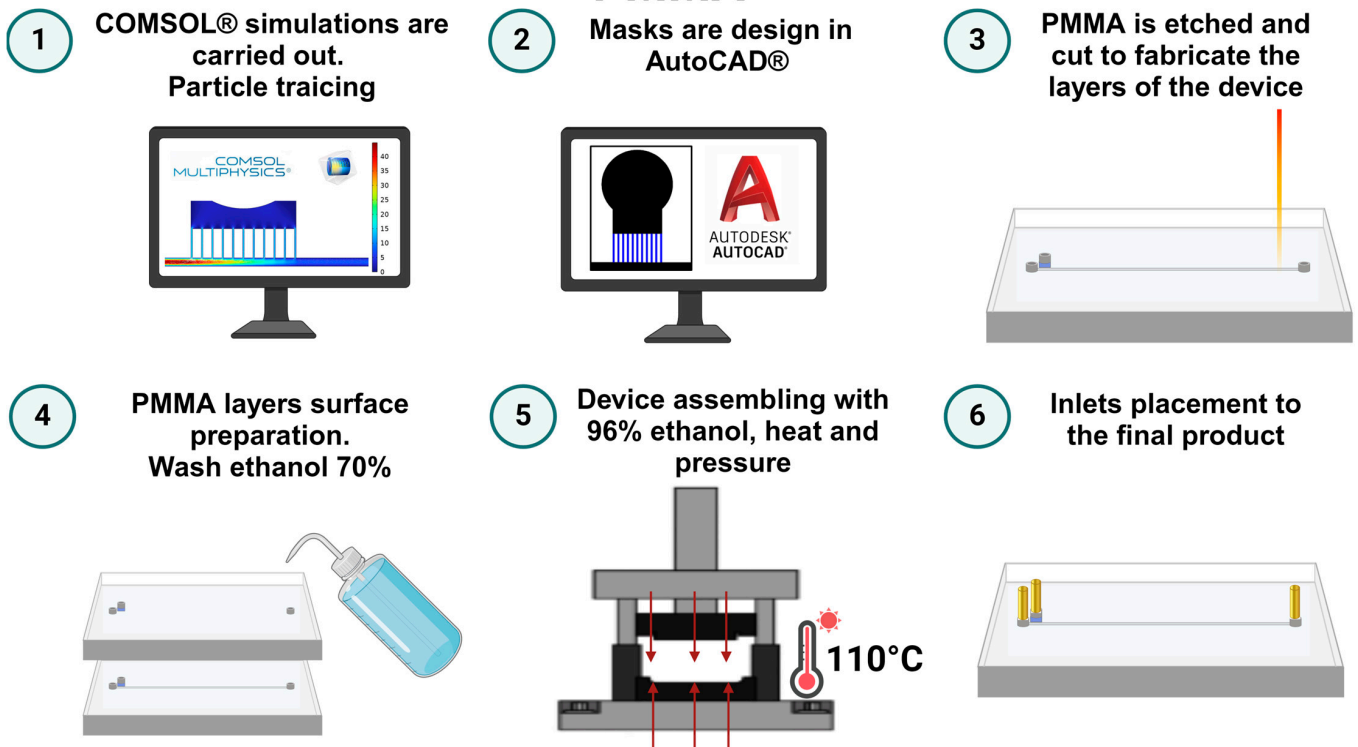


Figure 2. Manufacturing process of magnetic and Zweifach–Fung microfluidic devices via laser ablation in PMMA. The procedure begins with (1) computational design and simulation in COMSOL Multiphysics 6.2 software (COMSOL Inc., Stockholm, Sweden) to determine optimal geometry. The design is then (2) refined in AutoCAD, where engraving and cutting paths are precisely demarcated. (3) The PMMA sheets are accurately cut and engraved using a TROTEC® laser system (TROTEC, Marchtrenk, Austria) following the color-coded design specifications. (4) Post-ablation, the sheets are cleansed with ethanol to prepare the surfaces for bonding. (5) Sheets are fused under pressure and heat to form the microfluidic structure. (6) Inlets and outlets are integrated to finalize the device, making it ready for experimental application.

Table 1. Materials for the Manufacturing of the Microfluidic Device.

Material	Quantity	Cost per Unit (USD)	Total Cost (USD)
Microfluidic Connectors	3 units	USD 0.05	USD 0.15
PMMA Sheets (7.5 cm × 2.5 cm)	2 units	USD 0.26	USD 0.51
	1 mL	-	USD 0.071
	5 mL	-	USD 0.02
	1 mL	-	USD 0.069
Total cost			USD 0.82

2.6. Particle Synthesis for Assessing Device Performance

To comprehensively evaluate the performance of microfluidic separators, we synthesized chitosan microparticles and used commercial polystyrene particles (MV-F02, Microvec, Pińczów, Poland).

Microparticles of Chitosan

Chitosan microparticles were synthesized using a modified version of the protocol described by Rodríguez et al. [64]. Initially, the aqueous phase was prepared by dissolving 2% (*w/v*) chitosan in a 4% (*v/v*) acetic acid solution, stirred magnetically at 500 RPM for 24 h to ensure complete dissolution. Concurrently, the oil phase, composed of Tween 80 and mineral oil, was mixed to achieve a 2% (*v/v*) concentration.

After the preparation of both phases, 5 mL of the aqueous chitosan solution was gradually added to 100 mL of the oil phase. The mixture was then stirred at 600 RPM for 10 min using a Hei-TORQUE Precision 200 (Heidolph, Schwabach, Germany) mechanical stirrer to create a water-in-oil (W/O) emulsion. Following the emulsion formation, 1 mL of glutaraldehyde solution was added, and stirring continued at 300 RPM for an additional 2 h to promote cross-linking within the microparticles.

The chitosan microparticles were then isolated by centrifugation at 3600 RPM for 10 min and washed three times, first with hexane and subsequently with Type II water, to remove residual chemicals.

2.7. Experimental Separation Tests

2.7.1. Sensitivity Evaluation of the Passive Zweifach–Fung Microfluidic Devices

The sensitivity of the Passive Zweifach–Fung microfluidic device was assessed by evaluating its ability to correctly route commercial polystyrene microparticles labeled with rhodamine (B MV-F02, Microvec, Pińczów, Poland). Given that all microparticles involved in the test were smaller than 40 μm , they were expected to be channeled exclusively to outlet 1, following the device's design specifications.

During testing, microparticle solutions were introduced into the microfluidic device at total flow rates (TFRs) of 2, 20, and 200 mL/h using a KDS-100 syringe infusion pump from W.P. Instruments (Holliston, MA, USA). The experimental setup, including the infusion pump, is illustrated in Figure S3. The separation process was monitored, and microparticles were collected from two distinct outlets of the device—outlet 1 and outlet 2.

Each sample collected was analyzed using a spectrofluorometer (0239D-2219 FluoroMax plus C, Horiba, Kyoto, Japan) with the excitation wavelength set at 545 nm and emission measured at 560 nm. This facilitated quantification of microparticles from each outlet, allowing for an accurate assessment of the device's separation capabilities.

To analyze the results, particles detected in outlet 1 were expected, and their presence confirmed the device's functionality. Conversely, any microparticles found in outlet 2 were categorized as false negatives, indicating a failure in the device's ability to correctly separate and route particles smaller than 40 μm . The recall or sensitivity was calculated as the ratio of microparticles smaller than 40 μm correctly identified in outlet 1 compared to those smaller than 40 μm and collected in outlet 2. The separation performance was evaluated for 5 microfluidic chips to analyze the deviation and possible variations associated with the manufacturing technique.

2.7.2. Passive Chitosan Microparticle Separation

Performance comparison of the Passive Zweifach–Fung microfluidic against our previously utilized passive separation device was conducted using a standardized chitosan microparticle separation test as described in our earlier publication [64].

Initially, we introduced a solution containing chitosan microparticles into the Zweifach–Fung type passive separation device using a KDS-100 syringe infusion pump from W.P. Instruments (Holliston, MA, USA). The operational parameters, including the flow rate, were optimized based on the findings from experiments and simulations detailed in Figure 3. These results indicated that a flow rate of 2 mL/h is optimal for effective particle separation.

Samples of 1 mL were collected from each of the device's outlets and analyzed under an optical microscope (Primo Star, ZEISS, Jena, Germany) equipped with Zen 3.7[®] software (ZEISS, Jena, Germany). The analysis focused on determining the size distribution of the particles from each outlet.

Separation efficiency was evaluated as a binary separation task, with particles smaller than 40 μm classified as positive outcomes and those larger than 40 μm as negative outcomes. This binary approach provided a clear, quantifiable measure of the Zweifach–Fung device’s capabilities relative to our previous model, evaluating the parameters recall, precision, F1 score, and accuracy. The separation performance was evaluated for 5 microfluidic chips to analyze the deviation and possible variations associated with the manufacturing technique.

Recall was calculated as the ratio of true positives (particles smaller than 40 μm correctly identified in outlet 1) to the sum of true positives and false negatives (particles smaller than 40 μm incorrectly identified in outlet 2). This measure indicates the device’s ability to separate all relevant microparticles accurately.

Precision was determined as the ratio of true positives to the sum of true positives and false positives (particles larger than 40 μm incorrectly identified in outlet 1). This metric reflects the accuracy of the device in separating only the relevant microparticles without misclassifying larger particles.

F1 score, the harmonic mean of precision and recall, was used to provide a single measure of the device’s performance, balancing both false positives and false negatives. This score offers a comprehensive view of the device’s effectiveness in particle separation.

Accuracy was calculated as the ratio of correctly identified particles (both true positives and true negatives) to the total number of particles. This measure encompasses both its ability to correctly identify smaller particles and exclude larger ones.

3. Results and Discussion

3.1. Geometric Optimization of Passive Microfluidic Devices

The effectiveness of passive microfluidic systems is greatly influenced by flow dynamics, which are determined by the device geometries. In this study, we focused our investigation on optimizing the number of channels in Zweifach–Fung systems. This key design parameter significantly impacts the fluid dynamics and the efficiency of particle separation.

The computational study, leveraging a Lagrangian model within COMSOL Multiphysics 6.2 software (COMSOL Inc., Stockholm, Sweden), aimed to pinpoint the optimal number of microchannels for the efficient separation of particles averaging of 20 μm in size. These simulations depicted particle trajectories within a variety of microchannel arrangements and enabled a parametric analysis to quantify the system’s recall ability.

As depicted in Figure 3, part (a) shows simulated particle trajectories color-coded by size: blue for approximately 5 μm , green for 20 μm , and red for 40 μm . This color-coding clarifies how different-sized particles navigate the microchannels, providing insights into the system’s separation efficiency. Part (b) of Figure 3 displays a column graph illustrating the recall performance for configurations ranging from one to 12 microchannels. A clear trend emerges, showing that increasing the number of microchannels enhances recall efficiency, with an 11-channel design achieving a perfect recall rate of 100%.

Initial findings revealed that a single channel configuration resulted in a recall rate below 25%, setting a performance baseline. The introduction of additional channels markedly improved this rate, attributed to reduced fluid resistance within the microchannels compared to the main channel. Despite its wider cross-section, the main channel’s extended length increases fluid resistance, hindering particle flow. By increasing the number of microchannels, we effectively distributed the flow and minimized overall resistance, enhancing the lateral forces that direct particles toward the outlet more efficiently.

The 11-channel configuration, achieving the highest recall rate, was selected as the optimal design. This configuration was fabricated and subjected to extensive experimental testing and additional simulations to thoroughly understand its performance dynamics and operational characteristics under varying conditions. By leveraging the potential of employed multiphysics simulations, it was possible to reduce the extent of experimental testing, thereby lowering the experimental time [69,70].

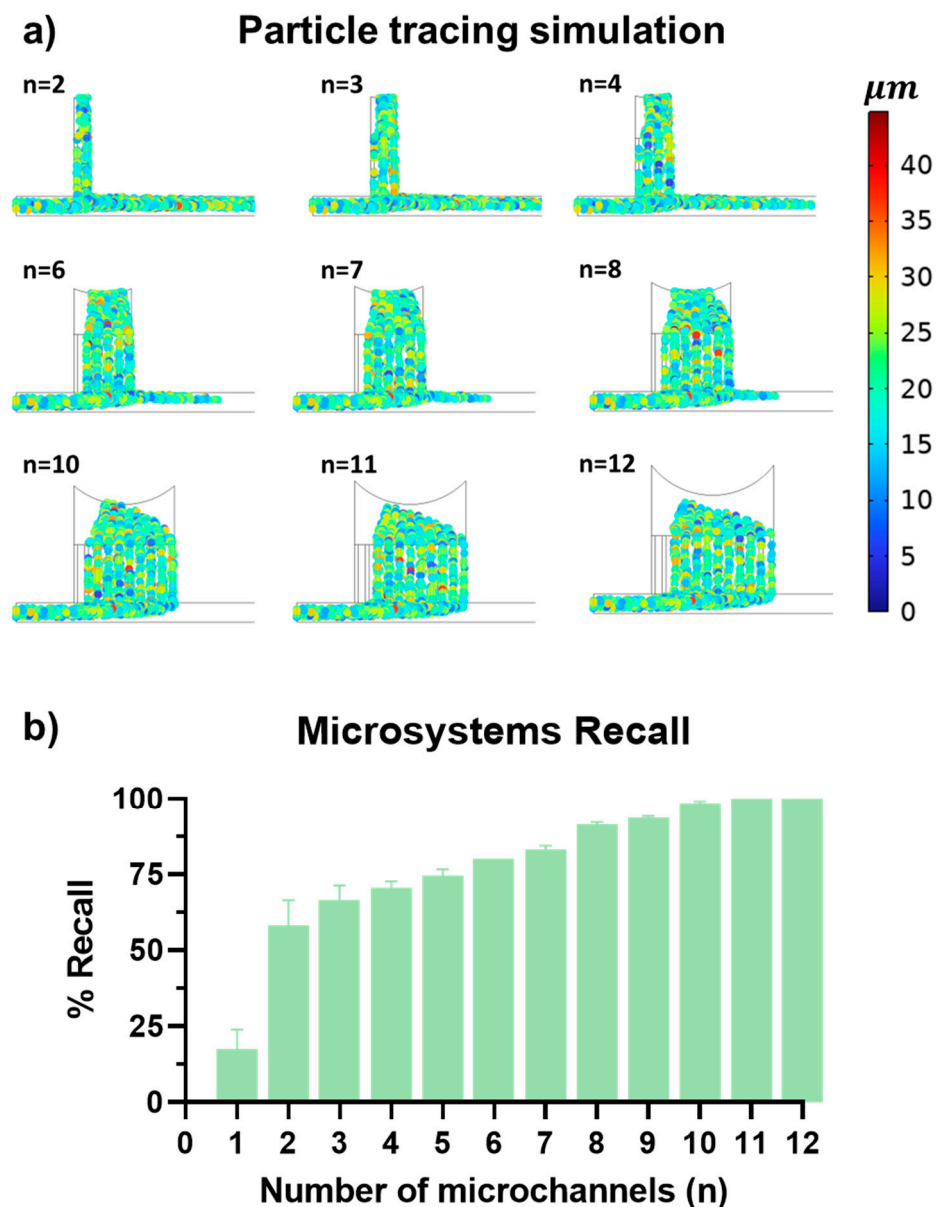


Figure 3. In silico evaluation of the recall efficiency in Zweifach–Fung microfluidic devices with multi-channels. (a) Particle trajectories: Color-coded simulation imagery depicting particle trajectories within microchannels. Colors represent particle sizes: blue for 5 μm , green for 20 μm (most prevalent), and red for 40 μm . This illustrates variations in flow dynamics and separation efficiency across different channel configurations. (b) Recall efficiency plot: Column plot displaying recall efficiency across varying numbers of microchannels from 1 to 12. A marked increase in efficiency is observed as the number of channels rises, with the configuration comprising 11 channels demonstrating the highest recall rate, identifying this as the optimal channel number.

3.2. Intrinsic Errors and Dimensional Reductions in PMMA Microfluidic Devices Fabricated by Laser Ablation

The low-cost manufacturing technique of laser ablation in PMMA inherently introduces errors, as documented in the existing literature [48]. Figure 4 presents a comparative analysis of the widths of 12 microfluidic channels measured both before and after the bonding process. Initially, these channels exhibit a mean width of $49.40 \mu\text{m} \pm 9.16 \mu\text{m}$. Following the bonding process, the mean width decreases to $44.85 \mu\text{m} \pm 8.27 \mu\text{m}$, representing an approximate reduction of 5 μm . This reduction is also accompanied by a noticeable

decrease in standard deviation. The elimination of channels exceeding 65 μm in width and the significant reduction in the occurrence of channels wider than 50 μm post-bonding, highlight the bonding process's impact on channel geometry.

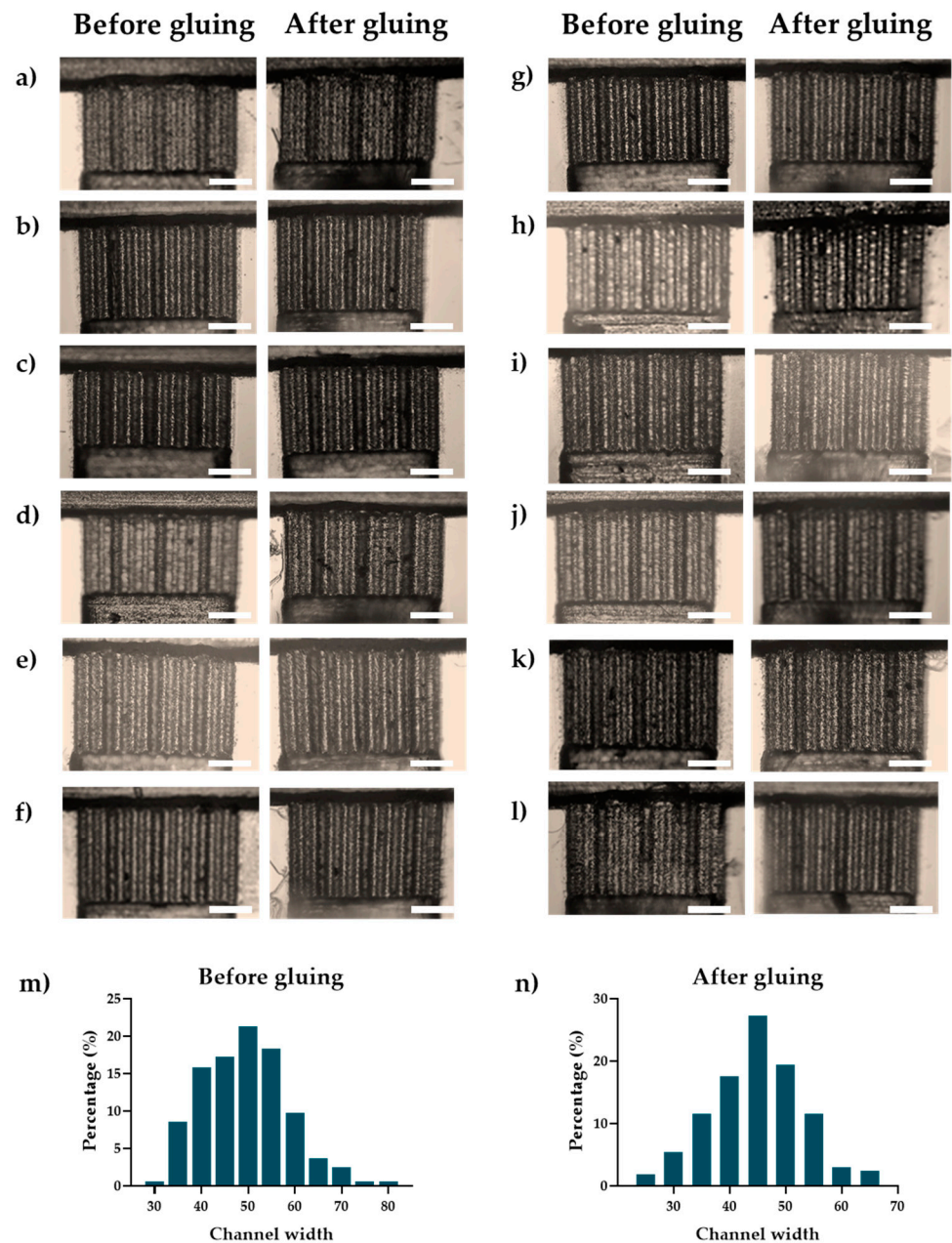


Figure 4. Microchannel before and after gluing. (a–l) Image collected by optical microscope before and after gluing with a $4\times$ objective. Scale bar 500 μm . (m) Channel width histogram before gluing. (n) Channel width histogram after gluing.

This observed narrowing effect is attributed to two primary factors: the Gaussian profile intrinsic to the laser ablation process, which contributes to initial dimensional variability, and the subsequent constriction during bonding, wherein ethanol-induced softening of the PMMA combined with applied compressive forces results in a consistent reduction in channel width [48]. These findings suggest that the bonding process not only reduces channel width but also enhances uniformity. This has significant implications for the performance of microfluidic devices, particularly in the context of particle separation, where diminished channel dimensions may restrict the range of particle sizes that can

be effectively processed. Subsequent sections will delve into the implications of these dimensional changes for the operational capabilities and efficiency of microfluidic chips.

3.3. TFR Impact on Zweifach–Fung (ZF) Microfluidic Device Performance

Following the geometric optimization of the Zweifach–Fung (ZF) microfluidic device, we evaluated its separation efficiency under various operational conditions. We utilized commercially available microparticles labeled with Rhodamine B to test the device’s performance, systematically varying the total flow rate (TFR) at 2, 20, and 200 mL/h to examine its impact on particle separation efficacy. The comparative results from both *in silico* predictions and experimental observations are compiled in Figure 5.

Microfluidic Recall Efficiency at Different Flow Rates

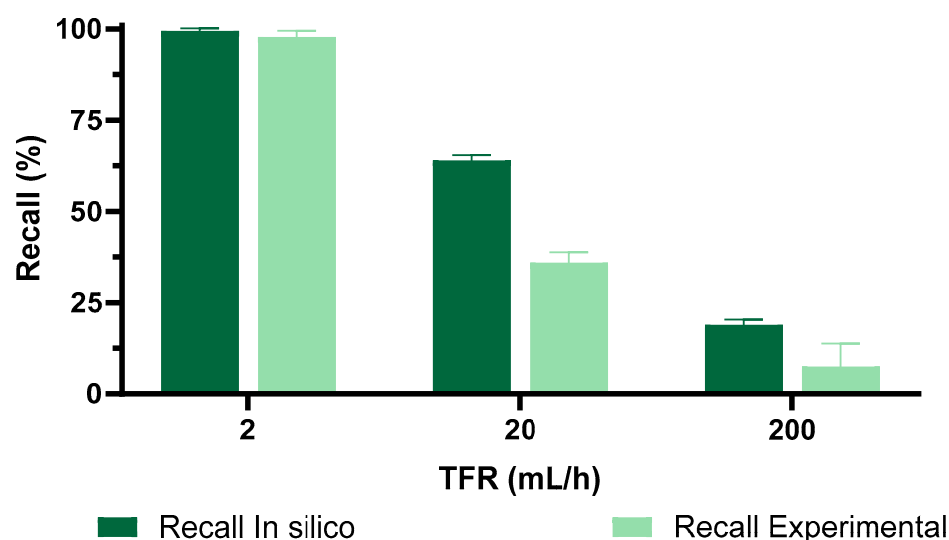


Figure 5. Comparison of recall efficiency between simulated and experimental results at varying TFRs: This section compares recall efficiencies as influenced by different total flow rates (TFRs), highlighting the impact of flow rate on separation performance and the discrepancies between simulated and actual experimental outcomes.

The data indicated that increasing TFRs detrimentally affected the separation efficiency. Both computational and experimental results confirmed this trend: higher TFRs led to more particles bypassing the intended bifurcations for separation. At the lowest TFR of 2 mL/h, the device demonstrated peak recall efficiency, achieving 100% recall. However, increasing the TFR to 20 mL/h resulted in a significant decrease in efficiency—experimental studies reported a recall rate of 45%, while simulations suggested a slightly higher rate of 65%. This disparity highlights the limitations of the computational model, which may not fully capture complex particle dynamics or subtle manufacturing nuances that become evident at higher flow rates.

At the highest TFR of 200 mL/h, efficiency plummeted to only 10% recall. This substantial decrease is attributed to the overwhelming influence of inertial forces at high fluid velocities, which override the device’s designed lateral forces that are crucial for size-based particle segregation. Consequently, the increased fluid velocity reduces the interaction time within the separation zones, diminishing the sorting mechanism’s effectiveness.

These findings, summarized in Figure 5, validate the importance of maintaining lower flow rates to achieve efficient particle separation within the ZF microfluidic design. The optimal flow rate of 2 mL/h was selected for subsequent device characterizations to ensure the most effective performance in practical applications. The deviations identified in the tests were 1.17 for the 2 mL/h test, 2.01 for the 20 mL/h test, and 4.48 for the 200 mL/h test.

These deviations are attributed to the manufacturing technique. As discussed in Section 3.1, this technique has an inherent error that causes variations in the microchannel dimensions.

3.4. Chitosan Particle Separation

Building upon the established optimal flow parameters, our study extended into a more sophisticated examination of the microfluidic device's capability, focusing not only on particle recall but also on precise separation and overall system accuracy.

Utilizing the chitosan microparticle separation protocol developed for and applied in the evaluation of a prior device [64], we conducted a series of tests to rigorously analyze the device's performance. The results are illustrated in Figure 6, where panel (a) details the particle distribution at outlet 1—intended for smaller particles—while panel (b) displays the distribution at outlet 2, expected to segregate larger particles. This dual-outlet analysis provided a nuanced understanding of the device's effectiveness across a range of particle sizes.

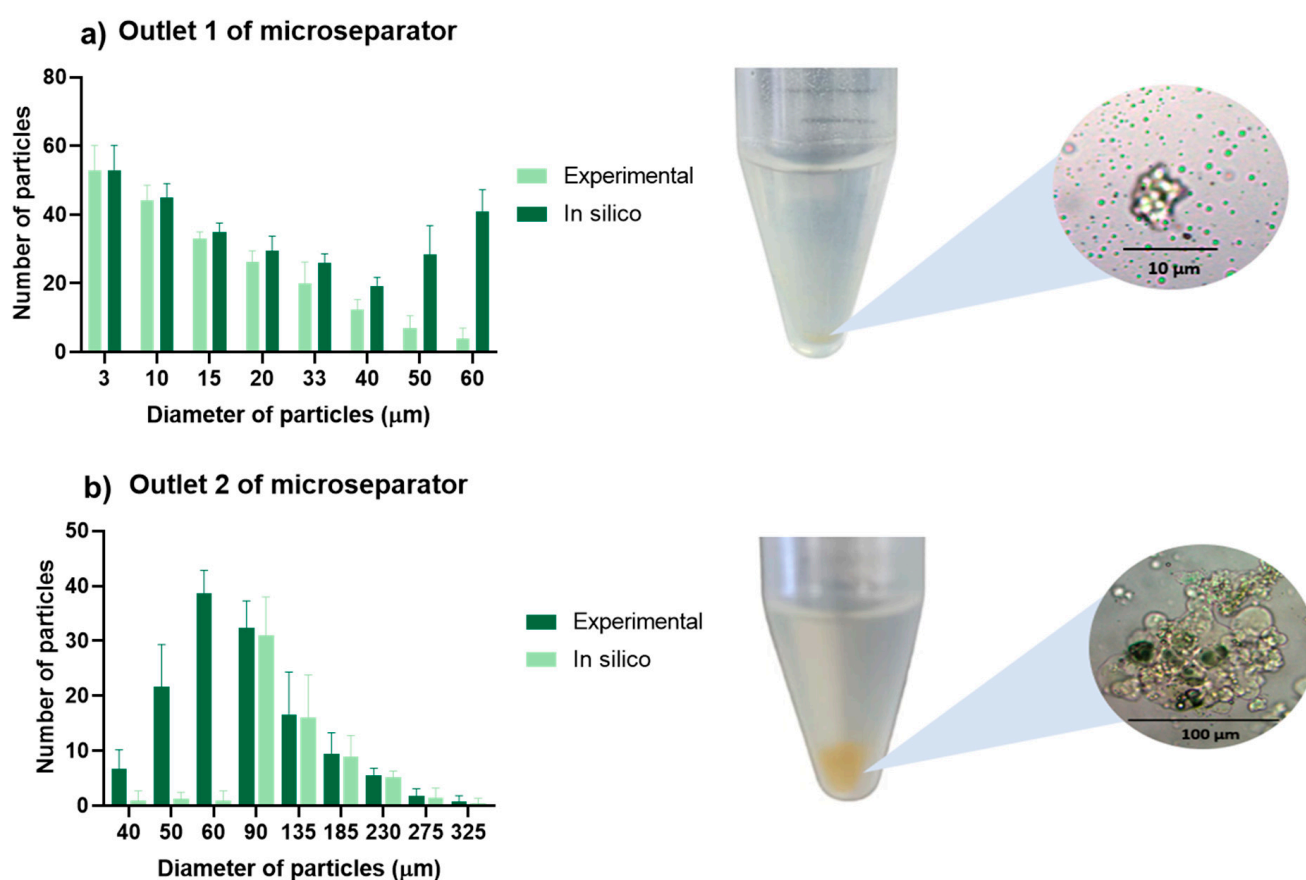


Figure 6. Chitosan microparticle separation performance in the Zweifach–Fung microfluidic device. (a) Distribution of particles at outlet 1, optimized for collecting particles under 40 μm; (b) particle distribution at outlet 2, designated for particles over 40 μm.

Under the optimal flow conditions identified in Figure 5, our comprehensive evaluation demonstrated exceptional efficiency in separating particles smaller than 40 μm, predominantly exiting through outlet 1. However, a significant deviation was observed with particles in the 50 to 60 μm range. The experimental recall rates here fell substantially short of the simulation predictions.

We hypothesize that this disparity may be due to partial blockages within the microchannels, a consequence of employing a low-cost laser ablation manufacturing process on PMMA. As illustrated in Figure 4 and corroborated by the literature, laser ablation, ethanol degradation, and the constriction effect generated during bonding results in a

reduction in the microchannel width from $49.40\ \mu\text{m} \pm 9.16\ \mu\text{m}$ to $44.85\ \mu\text{m} \pm 8.27\ \mu\text{m}$, corresponding to a reduction of $4.55\ \mu\text{m}$ in channel length. We associated this reduction in microchannel lengths with obstructions that impede the transport of larger particles, thereby diminishing the efficacy of the ZF separation channels for this particle size range.

To establish a baseline for comparison with prior research, we adhered to the same classification criteria as in our previous studies [68]. Particles with diameters less than $40\ \mu\text{m}$ were deemed positive, while those exceeding $40\ \mu\text{m}$ were classified as negative. This standardized metric ensured methodological consistency and enabled reliable assessment of the device's performance.

Our calculations revealed that the device achieved an average accuracy of $94.4\% \pm 3\%$ with a recall of $96.5\% \pm 3\%$. The precision stood at $94.5\% \pm 3\%$, and the F1 score—a measure that combines precision and recall—was $95.4\% \pm 3\%$. These robust figures underscore the exceptional capability of the ZF system to not only recall particles with high efficiency but also to do so with remarkable precision and reliability.

The performance metrics of the eleven-channel microfluidic device developed in this study were compared to other microfluidic systems documented in the literature, as detailed in Table 2. Our device manufactured using CO_2 laser ablation in PMMA presents the possibility of scaling up production at a cost of less than USD 0.90 per chip, and the manufacturing process takes only 15 min, which are important advantages for the device compared with the other microfluidic devices presented in the literature.

The efficiency of our device demonstrates favorable results when juxtaposed with other microfluidic technologies utilizing the ZF approach produced by alternative manufacturing processes. Our device shows comparable outcomes to other methodologies employed in similar microfluidic systems. Specifically, the precision of the ZF system maintained a high level of accuracy, aligning closely with the 96% precision reported in our previous study [68], indicating consistent reliability. Notably, there was a substantial improvement in recall performance, which increased from 77.62% in the earlier device to a significantly higher value in the current system. This enhancement in recall is further corroborated by the F1 score, which exhibited a notable rise from 79.70% to the present figure, underscoring the advancements achieved in the design and operational parameters of the current ZF system.

These results highlight the effectiveness of the improvements made to the ZF system and suggest that the advancements in this microfluidic device contribute to its superior performance compared to previously developed systems.

Table 2. Comparative Analysis of Microfluidic Devices in the Literature.

Literature	Our Work	[26]	[71]	[72]	[64]	[73]	[57]	[74]	[75]	[76]
Channel Geometry	T-shaped	U and W-shaped	Curved	T-shaped	Wave	Spiral-shaped	T-shaped	V complex-shaped	T and Y-shaped	T-shaped
Material	PMMA	PMMA	PDMS	PDMS	PMMA	PDMS	PMMA	PMMA	PDMS	PMMA
Fabrication Technique	CO ₂ laser	CO ₂ laser	Soft lithography	Photolithography	CO ₂ laser	Soft lithography	Soft lithography	Photolithography	Lithography	Lithography
Depth	60 µm	162–210 µm	40 µm	50 µm	-	-	-	20 µm	10 µm	20 µm
Channel Width	60 µm	180–227 µm	100–200 µm	300–700 µm	300 µm	15–40 µm	10–20 µm	9.6–15 µm	100 µm	
Cross Section	Gaussian	Gaussian	Gaussian	Rectangular	Gaussian	Rectangular	Rectangular	Gaussian	Rectangular	Rectangular
Flow Rate	2 mL/h	42 mL/h	-	-	23 mL/h	0.18–0.42 and 1.5–6 mL/h	6 mL/h	1–10 mL/h	0.01 mL/h	10 mL/h
Separation Technique	Zweifach–Fung effect	Hydrodynamic force	Centrifugal force, Coriolis force	Zweifach–Fung effect	Zweifach–Fung effect	Dean drag force	Zweifach–Fung effect	Plasma skimming effect	Zweifach–Fung effect	Zweifach–Fung effect
Cost per Chip	<USD 0.90	<USD 1.00	<USD 1.00	>USD 1.00	<USD 2.00	>USD 1.00	>USD 1.00	>USD 1.00	>USD 1.00	>USD 1.00
Fabrication Time	15 min	-	-	>1 h	15 min	>2 h	-	-	-	<1 h
Separation Efficiency	94%	92–96%	99%	99.70%	96.14%	8–13%	66.6%	65.1–100%	0.25	0.4
Particle Size	<40 µm	RBC size	RBC size	RBC size	15–40 µm	RBC size	RBC size	RBC size	8–16 µm	RBC size

3.5. SWOT Analysis (Strengths, Weaknesses, Opportunities, and Threats)

The novel Zweifach–Fung microfluidic device presented in this article demonstrates several key strengths, weaknesses, opportunities, and threats (SWOT) that merit consideration, as shown in Figure 7 [19]. One of the primary strengths of this device is its cost-effective manufacturing process. Utilizing a low-cost laser ablation method in PMMA reduces production costs to less than USD 0.90 and eliminates the need for cleanroom facilities. This affordability does not compromise performance, as the device achieves an overall accuracy of $94.4\% \pm 3\%$, indicating exceptional precision and recall. The use of Lagrangian computational simulations to optimize the eleven-channel Zweifach–Fung configuration further ensures high efficiency in particle separation. Additionally, the device maintains steady operational conditions, providing reliable and reproducible results that contrast favorably with traditional methods. Its versatility and reliability make it applicable across various fields where separate large amount of microparticles or microcapsules are necessary, including fields such as the food, pharmaceutical, oil and gas, and chemical industries, thereby promoting and accelerating the process and efficiency [77–82].

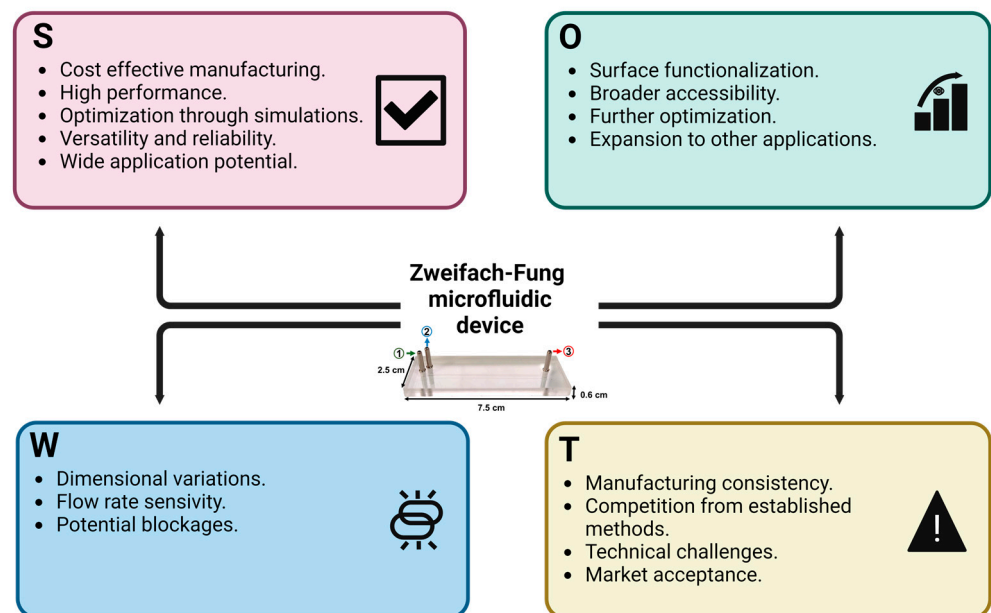


Figure 7. SWOT Analysis of the Zweifach–Fung Microfluidic Device. (S) Strengths, (W) weaknesses, (O) opportunities, and (T) threats.

However, the microfluidic device is not without its weaknesses. The manufacturing process introduces minor dimensional errors, reducing channel widths by approximately $5\ \mu\text{m}$ post-bonding, which could affect the performance. Additionally, the device's efficiency is highly sensitive to flow rates. Higher total flow rates significantly reduce separation efficiency, with a marked drop-in recall rate observed at increased flow rates. Furthermore, potential blockages due to sedimentation pose a challenge, potentially hindering consistent performance.

Despite these weaknesses, there are significant opportunities for improvement and broader applications. Future iterations of the device could incorporate surface functionalization techniques to minimize particle adhesion, thereby enhancing operational reliability [83–86]. The cost-effective nature of the device increases the accessibility of microfluidic technology, potentially leading to wider adoption and further innovation in the field. Additional research and development efforts could optimize the device's design and operational parameters, improving efficiency and reducing dimensional variability.

Nonetheless, the device faces several threats that could influence its widespread adoption. The inherent variability in the low-cost manufacturing process might lead to in-

consistencies in the device performance, affecting reliability. Competition from established microfluidic fabrication methods could limit the adoption of this new approach, particularly in industries where traditional methods are preferred. Continued technical challenges in ensuring precise control over channel dimensions and avoiding blockages could further impede widespread use. Lastly, market acceptance remains a potential threat; despite its advantages, the device may encounter resistance from industries accustomed to conventional methods, necessitating significant effort to demonstrate its efficacy and reliability.

4. Conclusions

This study conclusively demonstrates that an eleven-channel Zweifach–Fung microfluidic device configuration is essential for optimal particle recall, achieving 100% retrieval of particles conforming to a normal distribution with a mean diameter of 20 μm and a standard deviation of 6.7 μm . Through rigorous Lagrangian computational simulations, the research established 2 mL/h as the ideal operational flow rate, significantly enhancing the precision of particle separation to $94.4\% \pm 3\%$, a marked improvement from the previously recorded precision rate of 77.6% [64].

The study demonstrated a reduction in channels length by 4.55 μm , which was associated with the low-cost manufacturing processes employed, specifically laser ablation in the PMMA and the use of ethanol in the assembly. These processes likely alter the microchannel dimensions, subsequently impeding particle passage. This finding is crucial for the manufacturing of microfluidic devices with channels smaller than 100 μm using this low-cost approach. Therefore, it is recommended that future designs account for this reduction by developing microchannels 4.55 μm longer than initially planned to accommodate the manufacturing technique's inherent variation.

Moreover, despite the exceptional separation efficiency of the eleven-channel Zweifach–Fung device under optimal flow conditions, issues such as sedimentation leading to potential blockages were observed. Future iterations of the device design could benefit from integrating surface functionalization techniques to minimize particle adhesion, thus enhancing operational reliability while maintaining the cost-effectiveness of the fabrication process that eschews the need for cleanroom facilities. In sum, this research represents a substantial leap forward in the field of microfluidic separation technologies. The study not only underscores the capability of passive microfluidic devices to achieve high precision and reliability but also illustrates the feasibility of scaling such technologies through cost-effective manufacturing approaches. The Zweifach–Fung microfluidic device, with its refined design and optimized operational parameters, consistently delivered high accuracy, averaging 98% under ideal conditions, setting a new benchmark for performance in the realm of microfluidic applications.

Supplementary Materials: The following supporting information can be downloaded at: <https://www.mdpi.com/article/10.3390/mi15070932/s1>, Figure S1: Mesh convergence analysis; Figure S2: Close-up image of one of the fabricated microfluidic devices; Figure S3: Experimental setup employing the syringe infusion pump; Table S1: Properties of the simulated particles [64,87]; Table S2: Number of domain elements and boundary elements of the simulated microfluidics devices.

Author Contributions: Conceptualization, C.F.R., J.F.O. and J.C.C.; methodology, C.F.R. and M.B.-S.; software, C.F.R.; validation, C.F.R., J.F.O. and J.C.C.; formal analysis, C.F.R. and M.B.-S.; investigation, C.F.R. and M.B.-S.; resources, J.C.C.; data curation, C.F.R.; writing—original draft preparation, C.F.R. and M.B.-S.; writing—review and editing, J.C.C.; visualization, C.F.R. and M.B.-S.; supervision, C.M.-C., L.H.R., J.F.O. and J.C.C.; project administration, J.C.C.; funding acquisition, J.C.C. All authors have read and agreed to the published version of the manuscript.

Funding: The authors also would like to thank the Vice Presidency of Research & Creation's Publication Fund at Universidad de Los Andes for its financial support. Support by Minciencias Grant ID 624-2022 is gratefully acknowledged.

Data Availability Statement: The original contributions presented in the study are included in the article/Supplementary Materials; further inquiries can be directed to the corresponding author/s.

Acknowledgments: The Departments of Chemical and Food Engineering and Biomedical Engineering are gratefully acknowledged for providing access to their laboratories.

Conflicts of Interest: The authors declare no conflicts of interest.

References

- Wong, W.D.; Majnis, M.F.; Lai, C.W.; Sagadevan, S.; Muhd Julkapli, N. Enhancement of Mixing and Reaction Efficiency of Various Fluids Applications at Different Microfluidic Configuration and Design. In *Chemical Engineering and Processing—Process Intensification*; Elsevier: Amsterdam, The Netherlands, 2024. [\[CrossRef\]](#)
- Saxena, A.; Kumar, M.; Mishra, D.; Singh, K. Optimization of Newtonian Fluid Pressure in Microcantilever Integrated Flexible Microfluidic Channel for Healthcare Application. *Biomed. Phys. Eng. Express* **2024**, *10*, 035015. [\[CrossRef\]](#) [\[PubMed\]](#)
- Gurkan, U.A.; Wood, D.K.; Carranza, D.; Herbertson, L.H.; Diamond, S.L.; Du, E.; Guha, S.; Di Paola, J.; Hines, P.C.; Papautsky, I.; et al. Next Generation Microfluidics: Fulfilling the Promise of Lab-on-a-Chip Technologies. *Lab Chip* **2024**, *24*, 1867–1874. [\[CrossRef\]](#) [\[PubMed\]](#)
- Li, Z.; Ma, X.; Zhang, Z.; Wang, X.; Yang, B.; Yang, J.; Zeng, Y.; Yuan, X.; Zhang, D.; Yamaguchi, Y. A Rapid and Low-Cost Platform for Detection of Bacterial Based on Microchamber PCR Microfluidic Chip. *Biomed. Microdevices* **2024**, *26*, 20. [\[CrossRef\]](#) [\[PubMed\]](#)
- Mc Veigh, M.; Bellan, L.M. Microfluidic Synthesis of Radiotracers: Recent Developments and Commercialization Prospects. *Lab Chip* **2024**, *24*, 1226–1243. [\[CrossRef\]](#) [\[PubMed\]](#)
- Williams, D.E.; Li, W.; Chandrasekhar, M.; Corazza, C.M.O.W.; Deijs, G.S.; Djoko, L.; Govind, B.; Jose, E.; Kwon, Y.J.; Lowe, T.; et al. Lab on a Bead with Oscillatory Centrifugal Microfluidics for Fast and Complete Mixing Enables Fast and Accurate Biomedical Assays. *Sci. Rep.* **2024**, *14*, 8637. [\[CrossRef\]](#) [\[PubMed\]](#)
- Guan, Z.; Liu, Q.; Ma, C.-B.; Du, Y. Electrochemical Microfluidic Sensing Platforms for Biosecurity Analysis. *Anal. Bioanal. Chem.* **2024**, *1*, 1–15. [\[CrossRef\]](#) [\[PubMed\]](#)
- Rashidi, N.; Slater, A.; Peregrino, G.; Santin, M. A Novel, Microfluidic High-Throughput Single-Cell Encapsulation of Human Bone Marrow Mesenchymal Stromal Cells. *J. Mater. Sci. Mater. Med.* **2024**, *35*, 19. [\[CrossRef\]](#) [\[PubMed\]](#)
- Duarte, L.C.; Figueredo, F.; Chagas, C.L.S.; Cortón, E.; Coltro, W.K.T. A Review of the Recent Achievements and Future Trends on 3D Printed Microfluidic Devices for Bioanalytical Applications. *Anal. Chim. Acta* **2024**, *1299*, 342429. [\[CrossRef\]](#) [\[PubMed\]](#)
- Chavez-Pineda, O.G.; Rodriguez-Moncayo, R.; Gonzalez-Suarez, A.M.; Guevara-Pantoja, P.E.; Maravillas-Montero, J.L.; Garcia-Cordero, J.L. Portable Platform for Leukocyte Extraction from Blood Using Sheath-Free Microfluidic DLD. *Lab Chip* **2024**, *24*, 2575–2589. [\[CrossRef\]](#)
- Young, O.M.; Xu, X.; Sarker, S.; Sochol, R.D. Direct Laser Writing-Enabled 3D Printing Strategies for Microfluidic Applications. *Lab Chip* **2024**, *24*, 2371–2396. [\[CrossRef\]](#)
- Ortega Quesada, B.A.; Cuccia, J.; Coates, R.; Nassar, B.; Littlefield, E.; Martin, E.C.; Melvin, A.T. A Modular Microfluidic Platform to Study How Fluid Shear Stress Alters Estrogen Receptor Phenotype in ER + Breast Cancer Cells. *Microsyst. Nanoeng.* **2024**, *10*, 25. [\[CrossRef\]](#) [\[PubMed\]](#)
- Pan, P.; Qin, Z.; Sun, W.; Zhou, Y.; Wang, S.; Song, P.; Wang, Y.; Ru, C.; Wang, X.; Calarco, J.; et al. Correction: A Spiral Microfluidic Device for Rapid Sorting, Trapping, and Long-Term Live Imaging of Caenorhabditis Elegans Embryos. *Microsyst. Nanoeng.* **2023**, *9*, 147. [\[CrossRef\]](#) [\[PubMed\]](#)
- Gupta, P.; Mohan, A.; Mishra, A.; Nair, A.; Chowdhury, N.; Balekai, D.; Rai, K.; Prabhakar, A.; Saiyed, T. Multiplexed Fluorescence and Scatter Detection with Single Cell Resolution Using On-Chip Fiber Optics for Droplet Microfluidic Applications. *Microsyst. Nanoeng.* **2024**, *10*, 35. [\[CrossRef\]](#) [\[PubMed\]](#)
- Shan, H.; Sun, Q.; Xie, Y.; Liu, X.; Chen, X.; Zhao, S.; Chen, Z. Dialysis-Functionalized Microfluidic Platform for in Situ Formation of Purified Liposomes. *Colloids Surf. B Biointerfaces* **2024**, *236*, 113829. [\[CrossRef\]](#) [\[PubMed\]](#)
- He, G.; Pan, Y.; Zeng, F.; Qin, S.; Luan, X.; Lu, Q.; Xie, C.; Hu, P.; Gao, Y.; Yang, J.; et al. Microfluidic Synthesis of CuH Nanoparticles for Antitumor Therapy through Hydrogen-Enhanced Apoptosis and Cuproptosis. *ACS Nano* **2024**, *18*, 9031–9042. [\[CrossRef\]](#) [\[PubMed\]](#)
- Wang, W.; Wang, Y.; Zhang, D.; Guo, G.; Wang, L.; Wang, X. Kinetically Controlled Nucleation Enabled by Tunable Microfluidic Mixing for the Synthesis of Dendritic Au@Pt Core/Shell Nanomaterials. *Small* **2024**, *20*, 2302589. [\[CrossRef\]](#) [\[PubMed\]](#)
- Mehraji, S.; DeVoe, D.L. Microfluidic Synthesis of Lipid-Based Nanoparticles for Drug Delivery: Recent Advances and Opportunities. *Lab Chip* **2024**, *24*, 1154–1174. [\[CrossRef\]](#)
- Kulkarni, M.B.; Ayachit, N.H.; Aminabhavi, T.M.; Pogue, B.W. Recent Advances in Microfluidics-Based Paper Analytical Devices (MPADs) for Biochemical Sensors: From Fabrication to Detection Techniques. *Biochem. Eng. J.* **2023**, *198*, 109027. [\[CrossRef\]](#)
- Kang, K.; Lee, S.Y.; Kim, C.S.; Park, C.H. Hybrid Magnetic Field System with Helmholtz Coils and Magnets for Real-Time Circulating Tumor Cell Separation. *Sens. Actuators A Phys.* **2024**, *370*, 115229. [\[CrossRef\]](#)
- Xuan, Y.; Yin, M.; Sun, Y.; Liu, M.; Bai, G.; Diao, Z.; Ma, B. Magnetic Nanoparticle-Mediated Enrichment Technology Combined with Microfluidic Single Cell Separation Technology: A Technology for Efficient Separation and Degradation of Functional Bacteria in Single Cell Liquid Phase. *Bioresour. Technol.* **2024**, *401*, 130686. [\[CrossRef\]](#)
- Kutluk, H.; Viefhues, M.; Constantinou, I. Integrated Microfluidics for Single-Cell Separation and On-Chip Analysis: Novel Applications and Recent Advances. *Small Sci.* **2024**, *4*, 2300206. [\[CrossRef\]](#)

23. Peng, T.; Lin, X.; Li, L.; Huang, L.; Jiang, B.; Jia, Y. Investigation on Submicron Particle Separation and Deflection Using Tilted-Angle Standing Surface Acoustic Wave Microfluidics. *Heliyon* **2024**, *10*, e25042. [\[CrossRef\]](#)
24. Zhang, T.; Di Carlo, D.; Lim, C.T.; Zhou, T.; Tian, G.; Tang, T.; Shen, A.Q.; Li, W.; Li, M.; Yang, Y.; et al. Passive Microfluidic Devices for Cell Separation. *Biotechnol. Adv.* **2024**, *71*, 108317. [\[CrossRef\]](#) [\[PubMed\]](#)
25. Bagi, M.; Amjad, F.; Ghoreishian, S.M.; Sohrabi Shahsavari, S.; Huh, Y.S.; Moraveji, M.K.; Shimpalee, S. Advances in Technical Assessment of Spiral Inertial Microfluidic Devices Toward Bioparticle Separation and Profiling: A Critical Review. *Biochip J.* **2024**, *18*, 45–67. [\[CrossRef\]](#)
26. Ngum, L.F.; Matsushita, Y.; El-Mashtoly, S.F.; Fath El-Bab, A.M.R.; Abdel-Mawgood, A.L. Separation of Microalgae from Bacterial Contaminants Using Spiral Microchannel in the Presence of a Chemoattractant. *Bioresour. Bioprocess.* **2024**, *11*, 36. [\[CrossRef\]](#) [\[PubMed\]](#)
27. Karimi, A.; Sattari-Najafabadi, M. Numerical Study of Bacteria Removal from Microalgae Solution Using an Asymmetric Contraction-Expansion Microfluidic Device: A Parametric Analysis Approach. *Heliyon* **2023**, *9*, e20380. [\[CrossRef\]](#) [\[PubMed\]](#)
28. Fung, Y.C.; Zweifach, B.W. Microcirculation: Mechanics of Blood Flow in Capillaries. *Annu. Rev. Fluid Mech.* **1971**, *3*, 189–210. [\[CrossRef\]](#)
29. Petit, N. Control of a Microfluidic Separation Process Governed by the Zweifach-Fung Effect. *IFAC-Pap.* **2022**, *55*, 975–980. [\[CrossRef\]](#)
30. Bekiaris-Liberis, N.; Bresch-Pietri, D.; Petit, N. Compensation of Input-Dependent Hydraulic Input Delay for a Model of a Microfluidic Process under Zweifach–Fung Effect. *Automatica* **2024**, *160*, 111428. [\[CrossRef\]](#)
31. Lu, Y.; Shi, Z.; Yu, L.; Li, C.M. Fast Prototyping of a Customized Microfluidic Device in a Non-Clean-Room Setting by Cutting and Laminating Parafilm®. *RSC Adv.* **2016**, *6*, 85468–85472. [\[CrossRef\]](#)
32. Zhou, W.; Dou, M.; Timilsina, S.S.; Xu, F.; Li, X. Recent Innovations in Cost-Effective Polymer and Paper Hybrid Microfluidic Devices. *Lab Chip* **2021**, *21*, 2658–2683. [\[CrossRef\]](#)
33. Thomas, T.; Agrawal, A. Design and Fabrication of Microfluidic Devices: A Cost-Effective Approach for High Throughput Production. *J. Micromech. Microeng.* **2024**, *34*, 015008. [\[CrossRef\]](#)
34. Li, Y.; Wang, X.; Wang, Y.; Fan, Y. Low-Cost Hybrid Bonding between Thermoplastics and PDMS with Differential Adhesive Tape for Microfluidic Devices. *J. Mater. Sci. Mater. Electron.* **2023**, *34*, 565. [\[CrossRef\]](#)
35. Li, Y.; Wang, X.; Yang, S.; Liu, J.; Zhang, Q.; Fan, Y. Reversible Bonding of Thermoplastic-Based Microfluidics with Freeze-Release Adhesive. *Microfluid. Nanofluidics* **2023**, *27*, 33. [\[CrossRef\]](#)
36. Tsao, C.-W. Polymer Microfluidics: Simple, Low-Cost Fabrication Process Bridging Academic Lab Research to Commercialized Production. *Micromachines* **2016**, *7*, 225. [\[CrossRef\]](#) [\[PubMed\]](#)
37. Cong, H.; Zhang, N. Perspectives in Translating Microfluidic Devices from Laboratory Prototyping into Scale-up Production. *Biomicrofluidics* **2022**, *16*, 021301. [\[CrossRef\]](#)
38. Wang, Y.; Xu, F.; Fan, Y. Thermoplastic-Based Microfluidic Chip Bonding with PES Hot Melt Adhesive Film. *J. Adhes* **2024**, *100*, 178–185. [\[CrossRef\]](#)
39. Kaba, A.M.; Jeon, H.; Park, A.; Yi, K.; Baek, S.; Park, A.; Kim, D. Cavitation-Microstreaming-Based Lysis and DNA Extraction Using a Laser-Machined Polycarbonate Microfluidic Chip. *Sens. Actuators B Chem.* **2021**, *346*, 130511. [\[CrossRef\]](#)
40. Zhang, D.; Gao, R.; Huang, S.; Huang, Y.; Zhang, J.; Su, X.; Zhang, S.; Ge, S.; Zhang, J.; Xia, N. All-in-One Microfluidic Chip for 30-Min Quantitative Point-of-Care-Testing of Nucleic Acids. *Sens. Actuators B Chem.* **2023**, *390*, 133939. [\[CrossRef\]](#)
41. Madadi, M.; Madadi, A.; Zareifar, R.; Nikfarjam, A. A Simple Solvent-Assisted Method for Thermal Bonding of Large-Surface, Multilayer PMMA Microfluidic Devices. *Sens. Actuators A Phys.* **2023**, *349*, 114077. [\[CrossRef\]](#)
42. Persson, H.; Park, S.; Mohan, M.; Cheung, K.K.; Simmons, C.A.; Young, E.W.K. Rapid Assembly of PMMA Microfluidic Devices with PETE Membranes for Studying the Endothelium. *Sens. Actuators B Chem.* **2022**, *356*, 131342. [\[CrossRef\]](#)
43. Smith, S.; Sypabekova, M.; Kim, S. Double-Sided Tape in Microfluidics: A Cost-Effective Method in Device Fabrication. *Biosensors* **2024**, *14*, 249. [\[CrossRef\]](#) [\[PubMed\]](#)
44. Li, Q.; Jiang, B.; Li, X.; Zhou, M. Investigation of Solvent-Assisted In-Mold Bonding of Cyclic Olefin Copolymer (COC) Microfluidic Chips. *Micromachines* **2022**, *13*, 965. [\[CrossRef\]](#) [\[PubMed\]](#)
45. Srikantaprasad, G.; Mathew, N.T.; Nagar, S.V. Laser Micromachining on PMMA: An Efficient Fabrication of Microchannels for Sustainable Microfluidic Devices. *J. Braz. Soc. Mech. Sci. Eng.* **2024**, *46*, 325. [\[CrossRef\]](#)
46. Li, S.-C.; Chiang, C.-C.; Tsai, Y.-S.; Chen, C.-J.; Lee, T.-H. Fabrication of a Three-Dimensional Microfluidic System from Poly(Methyl Methacrylate) (PMMA) Using an Intermiscibility Vacuum Bonding Technique. *Micromachines* **2024**, *15*, 454. [\[CrossRef\]](#) [\[PubMed\]](#)
47. Ecker, R.; Mitteramskogler, T.; Fuchsluger, A.; Jakoby, B. Fabrication of an Ultrathin PMMA Foil for Sensing Applications in Microfluidic Systems. In Proceedings of the XXXV EUROSENSORS Conference, Lecce, Italy, 10–13 September 2023; p. 48. [\[CrossRef\]](#)
48. Anjum, A.; Azharuddin Ali, M.; Shaikh, A.A.; Akhtar, S.S. A Numerical and Experimental Analysis of CO₂ Laser Micro-Milling on PMMA Sheet Considering a Multipass Approach for Microfluidic Devices. *Opt. Laser Technol.* **2024**, *176*, 110860. [\[CrossRef\]](#)
49. Klank, H.; Kutter, J.P.; Geschke, O. CO₂-Laser Micromachining and Back-End Processing for Rapid Production of PMMA-Based Microfluidic Systems. *Lab Chip* **2002**, *2*, 242. [\[CrossRef\]](#) [\[PubMed\]](#)

50. Nasser, G.A.; Fath El-Bab, A.M.R.; Abdel-Mawgood, A.L.; Mohamed, H.; Saleh, A.M. CO₂ Laser Fabrication of PMMA Microfluidic Double T-Junction Device with Modified Inlet-Angle for Cost-Effective PCR Application. *Micromachines* **2019**, *10*, 678. [CrossRef] [PubMed]
51. Tweedie, M.; Maguire, P.D. Microfluidic Ratio Metering Devices Fabricated in PMMA by CO₂ Laser. *Microsyst. Technol.* **2021**, *27*, 47–58. [CrossRef]
52. Huang, T.-K.; Huang, C.-H.; Chen, P.-A.; Chen, C.H.; Lu, F.; Yang, W.-J.; Huang, J.Y.J.; Li, B.-R. Development of a Thermotaxis and Rheotaxis Microfluidic Device for Motile Spermatozoa Sorting. *Biosens. Bioelectron.* **2024**, *258*, 116353. [CrossRef]
53. Qin, L.; Yue, J.; Zhou, D.; Yang, A.; Zheng, S. Numerical and Experimental Study on the Synergistic Effect of Vortex and Contact Surface of Fluid in the Inlet Section of Micromixer. *Chem. Eng. Process.—Process Intensif.* **2024**, *196*, 109645. [CrossRef]
54. Yang, L.; Xu, F.; Chen, G. Effective Mixing in a Passive Oscillating Micromixer with Impinging Jets. *Chem. Eng. J.* **2024**, *489*, 151329. [CrossRef]
55. Su, W.; Han, B.; Yeboah, S.; Du, D.; Wang, L. Fabrication of Monodisperse Droplets and Microcapsules Using Microfluidic Chips: A Review of Methodologies and Applications. *Rev. Chem. Eng.* **2024**, *40*, 401–434. [CrossRef]
56. Ma, L.; Zhao, X.; Hou, J.; Huang, L.; Yao, Y.; Ding, Z.; Wei, J.; Hao, N. Droplet Microfluidic Devices: Working Principles, Fabrication Methods, and Scale-Up Applications. *Small Methods* **2024**. [CrossRef] [PubMed]
57. Shamsi, A.; Shamloo, A.; Mohammadaliha, N.; Hajghassem, H.; Mehrabadi, J.F.; Bazzaz, M. High Throughput Blood Plasma Separation Using a Passive PMMA Microfluidic Device. *Microsyst. Technol.* **2016**, *22*, 2447–2454. [CrossRef]
58. Bazaz, S.R.; Mehrizi, A.A.; Hesari, A.Z. A Novel Microfluidic Design for Blood Plasma Separation. In *Proceedings of the 2016 23rd Iranian Conference on Biomedical Engineering and 2016 1st International Iranian Conference on Biomedical Engineering (ICBME), Tehran, Iran, 24–25 November 2016*; IEEE: New York, NY, USA, 2016; pp. 97–101. [CrossRef]
59. Rodríguez, C.F.; Andrade-Pérez, V.; Vargas, M.C.; Mantilla-Orozco, A.; Osma, J.F.; Reyes, L.H.; Cruz, J.C. Breaking the Clean Room Barrier: Exploring Low-Cost Alternatives for Microfluidic Devices. *Front. Bioeng. Biotechnol.* **2023**, *11*, 1176557. [CrossRef] [PubMed]
60. Schneider, P.J.; Christie, L.B.; Eadie, N.M.; Siskar, T.J.; Sukhotskiy, V.; Koh, D.; Wang, A.; Oh, K.W. Pysanky to Microfluidics: An Innovative Wax-Based Approach to Low Cost, Rapid Prototyping of Microfluidic Devices. *Micromachines* **2024**, *15*, 240. [CrossRef]
61. Halwes, M.; Stamp, M.; Collins, D.J. A Rapid Prototyping Approach for Multi-Material, Reversibly Sealed Microfluidics. *Micromachines* **2023**, *14*, 2213. [CrossRef] [PubMed]
62. Li, Z.; Chen, L.; Ma, Y.; Weng, D.; Wang, Z.; Zhang, X.; Wang, J. Multi-Physics Coupling Simulation and Design of Magnetic Field-Driven Soft Microrobots in Liquid Environments. *Int. J. Mech. Sci.* **2024**, *272*, 109136. [CrossRef]
63. Rodríguez, C.F.; Ortiz, C.L.; Giraldo, R.K.A.; Munoz, C.C.; Cruz, J.C. In Silico Study of Spheroids Fusion through Magnetic Field Gradients. In *Proceedings of the 2021 IEEE 2nd International Congress of Biomedical Engineering and Bioengineering (CI-IB&BI), Bogota D.C., Colombia, 13–15 October 2021*; IEEE: New York, NY, USA, 2021; pp. 1–9. [CrossRef]
64. Rodríguez, C.F.; Guzmán-Sastoque, P.; Gantiva-Díaz, M.; Gómez, S.C.; Quezada, V.; Muñoz-Camargo, C.; Osma, J.F.; Reyes, L.H.; Cruz, J.C. Low-Cost Inertial Microfluidic Device for Microparticle Separation: A Laser-Ablated PMMA Lab-on-a-Chip Approach without a Cleanroom. *HardwareX* **2023**, *16*, e00493. [CrossRef]
65. Mumps, A. MULTifrontal Massively Parallel Sparse Direct Solve. Available online: <http://graal.ens-lyon.fr/MUMPS> (accessed on 1 February 2024).
66. Rodríguez-Soto, M.A.; Riveros-Cortés, A.; Orjuela-Garzón, I.C.; Fernández-Calderón, I.M.; Rodríguez, C.F.; Vargas, N.S.; Ostos, C.; Camargo, C.M.; Cruz, J.C.; Kim, S.; et al. Redefining Vascular Repair: Revealing Cellular Responses on PEUU—Gelatin Electrospun Vascular Grafts for Endothelialization and Immune Responses on in Vitro Models. *Front. Bioeng. Biotechnol.* **2024**, *12*, 1–26. [CrossRef] [PubMed]
67. Amestoy, P.R.; Duff, I.S.; L'Excellent, J.-Y.; Koster, J. MUMPS: A General Purpose Distributed Memory Sparse Solver. In *Proceedings of the 5th International Workshop, PARA 2000, Bergen, Norway, 18–20 June 2000*; Springer: Berlin/Heidelberg, Germany; pp. 121–130. [CrossRef]
68. Ortégón, S.; Peñaranda, P.A.; Rodríguez, C.F.; Noguera, M.J.; Florez, S.L.; Cruz, J.C.; Rivas, R.E.; Osma, J.F. Magnetic Torus Microreactor as a Novel Device for Sample Treatment via Solid-Phase Microextraction Coupled to Graphite Furnace Atomic Absorption Spectroscopy: A Route for Arsenic Pre-Concentration. *Molecules* **2022**, *27*, 6198. [CrossRef] [PubMed]
69. Keyes, D.E.; McInnes, L.C.; Woodward, C.; Gropp, W.; Myra, E.; Pernice, M.; Bell, J.; Brown, J.; Clo, A.; Connors, J.; et al. Multiphysics Simulations. *Int. J. High Perform. Comput. Appl.* **2013**, *27*, 4–83. [CrossRef]
70. Rodríguez, C.F.; Cruz, J.C. Critique—Simulation Apps. *Educ. Chem. Eng.* **2023**, *42*, 88–89. [CrossRef]
71. Zhang, J.; Guo, Q.; Liu, M.; Yang, J. A Lab-on-CD Prototype for High-Speed Blood Separation. *J. Micromech. Microeng.* **2008**, *18*, 125025. [CrossRef]
72. Tripathi, S.; Prabhakar, A.; Kumar, N.; Singh, S.G.; Agrawal, A. Blood Plasma Separation in Elevated Dimension T-Shaped Microchannel. *Biomed. Microdevices* **2013**, *15*, 415–425. [CrossRef] [PubMed]
73. Chávez Ramos, K.; Cañizares Macías, M.d.P. Microdevice Based on Centrifugal Effect and Bifurcation Law for Separation of Plasma from On-Line Diluted Whole Blood. *Anal. Bioanal. Chem.* **2021**, *413*, 5361–5372. [CrossRef] [PubMed]
74. Kersaudy-Kerhoas, M.; Kavanagh, D.M.; Dhariwal, R.S.; Campbell, C.J.; Desmulliez, M.P.Y. Validation of a Blood Plasma Separation System by Biomarker Detection. *Lab Chip* **2010**, *10*, 1587. [CrossRef]

75. Yang, S.; Ündar, A.; Zahn, J.D. A Microfluidic Device for Continuous, Real Time Blood Plasma Separation. *Lab Chip* **2006**, *6*, 871–880. [[CrossRef](#)]
76. Kersaudy-Kerhoas, M.; Dhariwal, R.; Desmulliez, M.P.Y.; Jouvét, L. Hydrodynamic Blood Plasma Separation in Microfluidic Channels. *Microfluid. Nanofluidics* **2010**, *8*, 105–114. [[CrossRef](#)]
77. de Souza, H.F.; dos Santos, F.R.; Cunha, J.S.; Pacheco, F.C.; Pacheco, A.F.C.; Soutelino, M.E.M.; Martins, C.C.N.; Andressa, I.; Rocha, R.d.S.; da Cruz, A.G.; et al. Microencapsulation to Harness the Antimicrobial Potential of Essential Oils and Their Applicability in Dairy Products: A Comprehensive Review of the Literature. *Foods* **2024**, *13*, 2197. [[CrossRef](#)]
78. Espinoza-Espinoza, L.A.; Muñoz-More, H.D.; Nole-Jaramillo, J.M.; Ruiz-Flores, L.A.; Arana-Torres, N.M.; Moreno-Quispe, L.A.; Valdiviezo-Marcelo, J. Microencapsulation of Vitamins: A Review and Meta-Analysis of Coating Materials, Release and Food Fortification. *Food Res. Int.* **2024**, *187*, 114420. [[CrossRef](#)] [[PubMed](#)]
79. Calderón-Oliver, M.; Ponce-Alquicira, E. The Role of Microencapsulation in Food Application. *Molecules* **2022**, *27*, 1499. [[CrossRef](#)] [[PubMed](#)]
80. Xu, X.; Tang, Q.; Gao, Y.; Chen, S.; Yu, Y.; Qian, H.; McClements, D.J.; Cao, C.; Yuan, B. Recent Developments in the Fabrication of Food Microparticles and Nanoparticles Using Microfluidic Systems. *Crit. Rev. Food Sci. Nutr.* **2024**, *64*, 1–15. [[CrossRef](#)] [[PubMed](#)]
81. Bolanos-Barbosa, A.D.; Rodríguez, C.F.; Acuña, O.L.; Cruz, J.C.; Reyes, L.H. The Impact of Yeast Encapsulation in Wort Fermentation and Beer Flavor Profile. *Polymers* **2023**, *15*, 1742. [[CrossRef](#)]
82. Ma, D.; Yang, B.; Zhao, J.; Yuan, D.; Li, Q. Advances in Protein-Based Microcapsules and Their Applications: A Review. *Int. J. Biol. Macromol.* **2024**, *263*, 129742. [[CrossRef](#)] [[PubMed](#)]
83. Xu, Z.; Jaiswal, A.; Liu, X.; Yang, Z.; Yin, Q.; Kong, K.V.; Yong, K. Microfluidics Evolution and Surface Functionalization: A Pathway to Enhanced Heavy Metal Ion Detection. *Adv. Sens. Res.* **2024**. [[CrossRef](#)]
84. Rohr, T.; Ogletree, D.F.; Svec, F.; Fréchet, J.M.J. Surface Functionalization of Thermoplastic Polymers for the Fabrication of Microfluidic Devices by Photoinitiated Grafting. *Adv. Funct. Mater.* **2003**, *13*, 264–270. [[CrossRef](#)]
85. Nielsen, J.B.; Hanson, R.L.; Almughamsi, H.M.; Pang, C.; Fish, T.R.; Woolley, A.T. Microfluidics: Innovations in Materials and Their Fabrication and Functionalization. *Anal. Chem.* **2020**, *92*, 150–168. [[CrossRef](#)]
86. Shakeri, A.; Jarad, N.A.; Khan, S.; F Didar, T. Bio-Functionalization of Microfluidic Platforms Made of Thermoplastic Materials: A Review. *Anal. Chim. Acta* **2022**, *1209*, 339283. [[CrossRef](#)]
87. Torres, C.E.; Cifuentes, J.; Gómez, S.C.; Quezada, V.; Giraldo, K.A.; Puentes, P.R.; Rueda-Gensini, L.; Serna, J.A.; Muñoz-Camargo, C.; Reyes, L.H.; et al. Microfluidic Synthesis and Purification of Magnetoliposomes for Potential Applications in the Gastrointestinal Delivery of Difficult-to-Transport Drugs. *Pharmaceutics* **2022**, *14*, 315. [[CrossRef](#)] [[PubMed](#)]

Disclaimer/Publisher’s Note: The statements, opinions and data contained in all publications are solely those of the individual author(s) and contributor(s) and not of MDPI and/or the editor(s). MDPI and/or the editor(s) disclaim responsibility for any injury to people or property resulting from any ideas, methods, instructions or products referred to in the content.